Applied Geochemistry 24 (2009) 936–949

Contents lists available at ScienceDirect

Applied Geochemistry

journal homepage: www.elsevier.com/locate/apgeochem

Estimating selenium removal by sedimentation from the Great Salt Lake, Utah

Wade Oliver [a,*], Christopher Fuller [b], David L. Naftz [c], William P. Johnson [a], Ximena Diaz [a,1]

[a] University of Utah, Department of Geology and Geophysics, Salt Lake City, UT 84112, USA
[b] US Geological Survey, 345 Middlefield Rd., Menlo Park, CA 94025, USA
[c] US Geological Survey, 2329 West Orton Circle, Salt Lake City, UT 84119, USA

ARTICLE INFO

Article history:
Received 10 September 2008
Accepted 16 February 2009
Available online 27 February 2009

Editorial handling by R. Fuge

ABSTRACT

The mass of Se deposited annually to sediment in the Great Salt Lake (GSL) was estimated to determine the significance of sedimentation as a permanent Se removal mechanism. Lake sediment cores were used to qualitatively delineate sedimentation regions (very high to very low), estimate mass accumulation rates (MARs) and determine sediment Se concentrations. Sedimentation regions were defined by comparison of isopach contours of Holocene sediment thicknesses to linear sedimentation rates determined via analysis of ^{210}Pb, ^{226}Ra, ^{7}Be and ^{137}Cs activity in 20 short cores (<5 cm), yielding quantifiable results in 13 cores. MARs were developed via analysis of the same radioisotopes in eight long cores (>10 cm). These MARs in the upper 1–2 cm of each long core ranged from 0.019 to 0.105 $g_{sed}/cm^2/a$. Surface sediment Se concentrations in the upper 1 or 2 cm of each long core ranged from 0.79 to 2.47 mg/kg. Representative MARs and Se concentrations were used to develop mean annual Se removal by sedimentation in the corresponding sedimentation region. The spatially integrated Se sedimentation rate was estimated to be 624 kg/a within a range of uncertainty between 285 and 960 kg/a. Comparison to annual Se loading and other potential removal processes suggests burial by sedimentation is not the primary removal process for Se from the GSL.

1. Introduction

The Great Salt Lake (GSL) is a terminal lake located in northern Utah. To the east are the Wasatch Mountains representing the western extent of the Rocky Mountains. To the west is the Basin and Range province of the western USA that is characterized by extensional stress and a horst and graben landscape. The GSL resides in two distinct depressions and covers an area of about 4400 km^2 (Stokes, 1980). The south arm of the lake (defined below) contains the Carrington and East Lake Faults (Colman et al., 2002).

The GSL is well-known as a remnant of Pleistocene Lake Bonneville that occupied much of western Utah and stretched into Nevada and Idaho. The current geochemistry of the lake is partly a result of the evaporation of this system and partly a result of the dissolved solid load of riverine inflows (Stokes, 1980). The current GSL is a Na–Cl brine that is 3–5 times more saline than the ocean, but with a similar geochemical composition (Sturm, 1980).

Construction of a rock-filled railroad causeway in 1959 divided the lake into two distinct, hydraulically separated bodies of water. The south arm, receiving the majority of freshwater inflows, has a higher water level and is less saline than the north arm (Sturm, 1980). The south arm is also stratified with a deep brine layer occupying the lower portion of the water column below approximately 6 m depth. The deep brine layer, though semi-transient in presence and depth (Gwynn, 2002), is an anoxic, dense brine with high levels of SO_4 reduction resulting in high sulfide concentrations (Domagalski, 1988). This deep brine layer has been thought to induce the geochemical precipitation of trace elements entering the lake to sediment by immobilization in sulfides to the point of being a "self-cleaning system" (Tayler et al., 1980).

Due to the terminal nature of the GSL, trace elements that have entered the lake cannot be flushed downstream and must be removed from the water column by other mechanisms. Previous studies have shown that volatilization to the atmosphere can be a significant removal mechanism for trace elements in some water bodies (Nriagu, 1989; Amouroux and Donard, 1996) by conversion into volatile forms, e.g. through a biologically mediated methylation process (Amouroux and Donard, 1997). Permanent sedimentation due to geochemical precipitation in the deep brine layer and to the settling of particulate matter represents another potentially significant removal mechanism for trace elements entering the GSL (Tayler et al., 1980).

Selenium is a trace element of interest due to the recent concerns over the effects of elevated Se loads on birds. Selenium is a required micronutrient for many animals, including endemic and migratory waterfowl and other birds that are found at the GSL. It

* Corresponding author. Present address: Texas Water Development Board, P.O. Box 13231, 1700 N. Congress Ave, Austin, TX 78711, USA. Tel.: +1 512 463 3132; fax: +1 512 936 0889.
E-mail address: wadeoliver@gmail.com (W. Oliver).
[1] Present address: Department of Extractive Metallurgy, Escuela Politécnica Nacional, Quito, Ecuador.

0883-2927/$ - see front matter © 2009 Elsevier Ltd. All rights reserved.
doi:10.1016/j.apgeochem.2009.02.023

is unique because the level of exposure that is toxic to birds is not much greater than the nutritional requirement (Seiler et al., 2003). High levels of Se in water have been shown to lead to death and malformations in bird embryos and chicks (Ohlendorf, 2003; Heinz, 1996).

As part of a US Department of the Interior (DOI) study under the National Irrigation Water Quality Program (NIWQP), Se levels and effects on birds were investigated at 26 sites across the western USA. Results showed that over 40% of bird eggs collected had Se concentrations above the 6 mg/kg threshold for reduced hatchability (Seiler et al., 2003).

In order to protect the large numbers and many species of migratory birds that rely on the GSL, it is important to understand the cycling of Se in the lake. Up to 1.5 million Eared Grebes molt on the GSL each year (Aldrich and Paul, 2002). The GSL also hosts the largest population of Wilson's Phalarope in the world with over 500,000 individuals migrating through annually (Shussman, 1999). Significant populations of many other species of birds such as American Avocet, White Pelican and Black-Necked Stilt also rely on the GSL (Shussman, 1999; Keith, 2005).

The role of sedimentation as a removal mechanism for Se in the GSL has not been previously studied. However, there have been multiple investigations of other trace elements in sediment in and around the GSL. Domagalski (1988) investigated the concentrations of trace elements at three sites in the GSL representing over 1 ka of accumulation. However, the resolution of these cores both spatially and with depth was not sufficient for use in interpreting sediment trace element concentrations across the entire lake and for the period subsequent to the construction of the railroad causeway.

Another set of cores collected in Farmington Bay in 1998 were analyzed for both sedimentation rate and selected trace element concentrations (Mahler et al., 2006; Naftz et al., 2000). Though this information is useful in reconstructing historical changes in the loading of trace elements to the GSL, the salinity of Farmington Bay is much lower than that of the main body of the GSL and the sedimentation characteristics are not likely representative of the lake as a whole. Additionally, neither of the above coring investigations included Se as part of the analyses.

The concentration of trace elements in sediment is not the only important factor in determining their removal to sediment. Sedimentation rates must also be determined. One source of information on sedimentation rates at the GSL is the thickness of sediment deposited during the Holocene Epoch as described in Colman et al. (2002) and Dinter (2007). In general, Holocene sediment thicknesses are high along the fault slightly west of the western shore of Antelope Island (Fig. 1). East of this line, Holocene thickness decreases dramatically. West of the fault, sediment thickness declines more slowly and continues to decline to the western shore of the south arm of the GSL. In the north basin of the south arm, Holocene sediment thicknesses are highest along the Carrington fault and near the railroad causeway and decrease slowly toward the SW to the shore. Sediment focusing – the preferential deposition of sediments and associated contaminants at a site from both the redistribution of sediments from within the lake and from sediments delivered from the watershed (Van Metre and Fuller, 2009) – likely played a large role in determining this distribution of Holocene sediment thicknesses exhibited by the strong apparent relationship with lake depth (Colman et al., 2002; Baskin, 2005). Due to the change in the geochemistry of the lake as a result of the construction of the railroad causeway, however, the sedimentation rates since 1959 may be significantly different than the average rate during the Holocene.

This investigation sought to estimate the contemporary annual mass of Se removed to sediment from analysis of lake-core sediments. This analysis included the characterization of Se concentrations and radioisotope activity, the spatial integration of these results into a Se removal estimate, and an assessment of the uncertainty in the resulting estimate. This research was performed concurrently and collaboratively with other investigations to better understand Se cycling processes at the GSL. An estimate of Se loaded to the GSL by rivers and the concentration of Se in the water column throughout the study period is presented in Naftz et al. (2009). An estimation of the mass of Se removed annually to the atmosphere by volatilization is given in Diaz et al. (2009). The transfer of Se from the water phase to biota has also been investigated (Wurtsbaugh, 2007). The end goal of this and the other Se cycling investigations is to assist in the development of an enforceable, numeric water quality standard that will protect current and future beneficial uses of the GSL.

2. Methodology

2.1. Sediment core collection

The focus area of this investigation is the south arm of the GSL, often referred to as Gilbert Bay (Fig. 1). The vast majority of riverine inputs to the GSL flow directly or indirectly into the south arm (Tayler et al., 1980). The south arm is defined as the lake area (exclusive of solar evaporation ponds and Farmington Bay) south of the railroad causeway (Baskin, 2005). At the historical average lake surface elevation of 1280 m above sea level, the south arm accounts for approximately 47% of the total lake area (Baskin, 2005).

Lake cores were taken at various sites in the south arm of the GSL (Fig. 1). Short cores (<5 cm) were collected at 20 sites during June 2007 using a 14 cm square box coring device which was lowered gently to the lake bottom from a boat using a hydraulic winch. Short cores were sectioned into two intervals, 0–1 cm and 4–5 cm, for analysis in order to efficiently determine sites on the lake suitable (i.e. with a quantifiable sedimentation rate) for the collection of the longer cores in July 2007.

Long core sediments were collected at three sites during July 2006 and at five sites during July 2007 (Fig. 1). The locations of the five long cores collected in 2007 were determined using the short core sedimentation rates to ensure an adequate spatial distribution of the long cores and that recent sedimentation had occurred in these locations. The upper 20 cm of each of the long cores was sectioned in situ into 1- or 2-cm increments within 6 h of collection. Core slices were then chilled on ice prior to freeze-drying.

With the exception of site 3510, a gravity coring device was used to collect all long cores. The 6.7-cm diameter gravity coring device was lowered slowly through the water column until it was about 1 m above the lake bottom, at which point it was released to free-fall into the sediment. The core at site 3510 was collected using a box corer, as described for the short cores above, to minimize compaction and provide the best possible determination of age as a function of depth (and sedimentation rate) in the shallowest sediment. Use of the gravity corer was chosen as the primary coring method, however, in order to collect deeper sediment profiles.

2.2. Chemical analysis of sediment cores

All core slices were freeze-dried, ground with a clean ceramic mortar and pestle and homogenized by mechanical mixing. Weights before (wet) and after (dry) freeze-drying were recorded. Sediment bulk density (g dry sediment/cm^3 of wet sediment) was determined for each core interval by volumetric displacement of dry sediment. Dry sediment was placed in a tared 10-mL volumetric flask, weighed and filled to the mark with deionized water. After

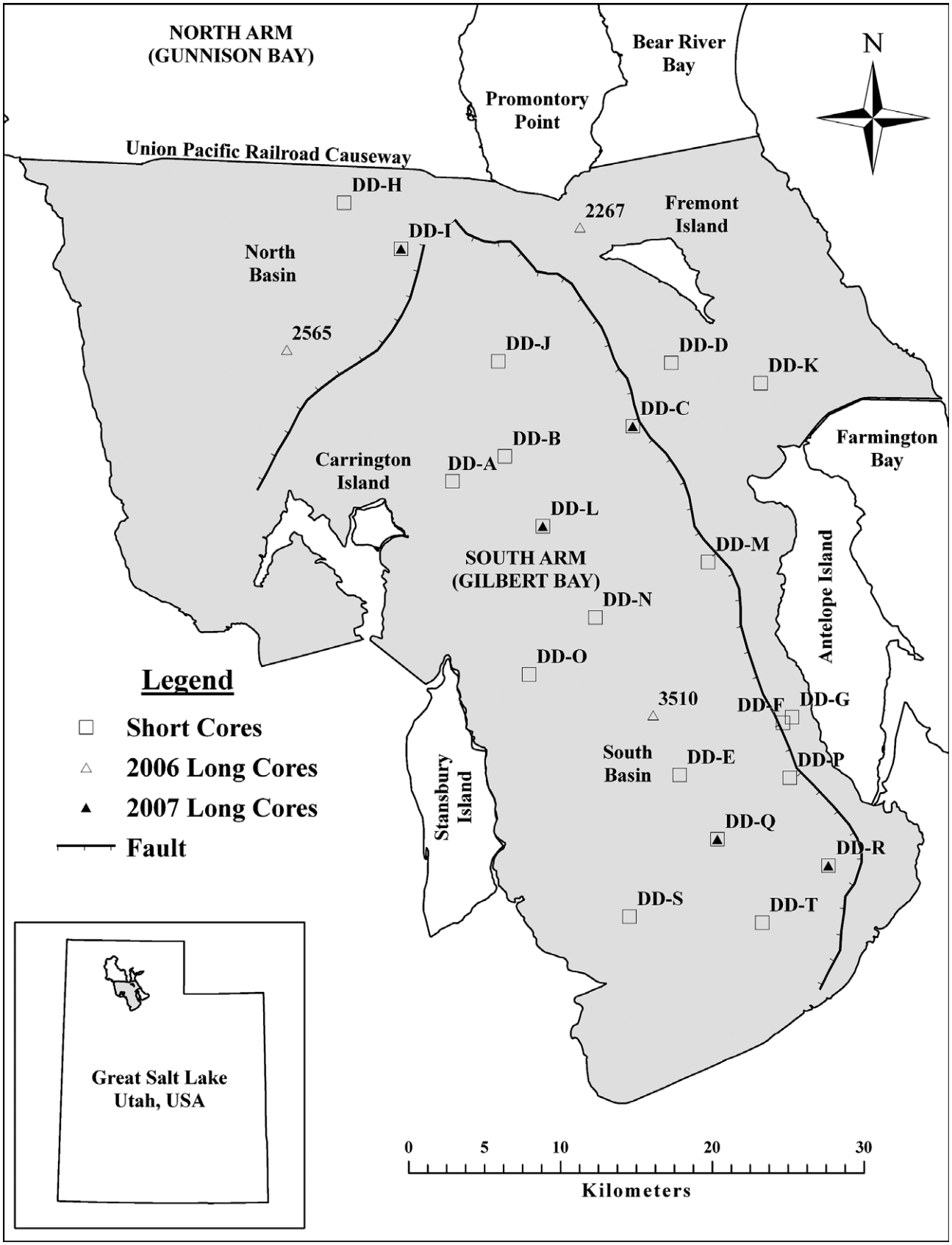

Fig. 1. Core locations in the south arm of the Great Salt Lake.

24 h, additional water was added as required and the final weight was recorded, with the volume of water added equal to the difference in weight. Because of the very high pore water salinity of Great Salt Lake sediments, the salt content of dried sediments (up to 40%) varies with porosity and must be accounted for. Therefore, the density of a subsample of the solution in the volumetric flask for each interval was measured using an Anton Paar DMA 35n portable density meter. The difference in density between solution and deionized water was attributed to weight of salt dissolved and was used to calculate the salt weight fraction of the dry sediment added to the flask. The salt-free sediment dry weight density was determined by dividing the salt-free dry weight by the volumetric difference between the flask and the volume of water added. Sediment bulk densities ranged from 1.3 to 2.3 g/cm^3 and increased with depth, likely due to degradation of organic matter. The fractional salt weight was used to correct measured radioisotope activities and Se to concentration/g of salt-free sediment.

In the eight long cores, one fraction of each core interval was analyzed for Se by hydride generation – atomic absorption spectrometry at Laboratory and Environmental Testing, Inc. (LET; Columbus, MO). The freeze-dried core fractions were digested using the L5-magnesium dry ash digestion procedure in which the Se was extracted from the sediment using a prescribed application of $MgNO_3{\cdot}6H_2O$, HNO_3, HCl and heat. The lower reporting limits for Se ranged from 0.2 to 0.4 mg/kg.

The measured sediment Se concentrations required correction for salt content. The mass of salt and the contribution of dissolved Se in pore water from the drying process were accounted for using the following equation to yield the salt-corrected Se concentration in the sediment:

$$[Se_{sed}] = \frac{[Se_{dry}] - \frac{Mass_{salt}}{Mass_{dry}} \times [Se_{salt}]}{\frac{Mass_{dry} - Mass_{salt}}{Mass_{dry}}} \quad (1)$$

where $[Se_{dry}]$ is the concentration of Se in the dry sample, $Mass_{salt}$ is the mass of salt calculated from the measured salt fraction and the dry mass, $Mass_{dry}$ is the total dry mass of the sample, $[Se_{salt}]$ is the Se concentration in the salt calculated from the percent salinity and the average total Se concentration in the water column, and $[Se_{sed}]$ is the Se concentration in the sediment corrected for salt content. The average total Se concentration in the water column (0.68 μg/L) is the average of 48 samples collected around the south arm from May 2006 through August 2007. The percent salinity of the pore water in each of the cores was calculated from the mass of salt in the core slice and the mass of water removed (wet minus dry weight). Salinities ranged from 9.1% to 16.3% with a mean of 12.6%. Salt-corrected Se concentrations for the core intervals used in this investigation are shown in Table 1.

A second fraction of the freeze-dried core slices was analyzed for radioisotopes to estimate the rate of sediment deposition. The measured radioisotope activities were also corrected for salt content of dry sediments using a similar approach but without correction for pore water radionuclide in the dried salt, which are assumed to be negligible. To account for compaction when determining sediment mass accumulation rates (MARs) in the long cores, it was necessary to determine the cumulative dry mass at the midpoint in each core slice. The dry mass of sediment in these samples – the mass of sediment after salinity correction per unit area in each core slice – was established using the method described in Van Metre et al. (2004) in which the porosity of dry sediment was estimated from the wet and dry weights and the measured bulk density. The cumulative dry mass of sediment was then determined as the sum of dry masses, corrected for salt content, above the midpoint of a particular core slice.

Core shortening, the loss of sediment mass loss from thinning of sediment layers has been observed during operation of gravity corers and is attributed to frictional resistance along the core barrel pushing a fraction of sediments away from the corer instead of into the sampler (Blomqvist, 1985; Crusius and Anderson, 1991). Because sediment MAR and Se deposition rates are determined from integrated sediment mass and concentrations, the potential loss of sediment mass due to core shortening during gravity core collection must be evaluated and accounted for. The extent of core shortening was estimated for site 3510 by comparing gravity core profiles of water content and porosity versus cumulative sediment dry mass to box core profiles, assuming the box core collects undisturbed sediment profiles (Blomqvist, 1985; Van Metre et al., 2004). These parameters were offset by about 1.5 cm in the gravity core compared to the box core which is likely the result of core shortening mass loss in the upper few cm of the gravity core. Using an iterative approach, sediment dry mass was added to the upper sediment intervals until the gravity core profile matched the box core. The best match required increasing the dry mass of each of the top four 1-cm intervals of the gravity core profile by 0.1 g/cm^2, and resulted in a fractional loss in dry mass that decreased from 70% to 30% with increasing depth. The dry mass (g/cm^3) of each of the other gravity cores was increased by this proportion over the upper 4 cm, assuming that the core shortening was proportional to the estimate for site 3510 gravity core. The

Table 1
Long core analysis results for surface interval mass accumulation rate (MAR) and sediment Se concentration. Also reported are the assigned sedimentation zone, deposition date range of the surface interval, percent salinity of pore water and MAR for the whole core.

Site ID	Depth interval (cm)	Sedimentation zone	Surface MAR (g/cm^2/a)	Se conc. (mg/kg)	Date of top	Date of bottom	Whole core MAR (g/cm^2/a)	Percent salinity (%) (w/w)
3510	0–1	Low	0.054	1.58	2006	2005	0.037	11.1
3510	1–2			2.01	2005	2000		10.7
2565	0–2	Very low	0.000	0.79	N/A	N/A	0	15.2
2267	0–2	Low	0.000	1.00	N/A	N/A	0	9.1
DD-C	0–1	High	0.105	1.67	2007	2005	0.038	11.2
DD-C	0–2			1.60	2005	2002		11.1
DD-I	0–1	High NW	0.105	0.97	2007	2005	0.038	13.3
DD-I	0–2			1.12	2005	2003		11.1
DD-L	0–1	Medium	0.044	1.85	2007	2001	0.016	12.0
DD-L	0–2			2.00	2001	1991		13.2
DD-Q	0–1	Low	0.019	2.46	2007	1991	0.013	12.0
DD-R	0–1	Medium	0.061	1.08	2007	2004	0.021	9.4
DD-R	0–2			1.90	2004	1998		11.6

resulting core shortening corrected interval masses were used for subsequent calculations.

The 0–1 and 4–5 cm intervals from the 20 short core samples were analyzed for ^{210}Pb, ^{226}Ra, ^{137}Cs and ^{7}Be by gamma spectrometry at the USGS Sediment Radioisotope Laboratory in Menlo Park, CA, as described in Van Metre et al. (2004). Age-dating of the lake sediments is possible because ^{210}Pb is produced in the atmosphere by decay of Rn, having a half-life of 22.3 a. Atmospheric deposition of ^{210}Pb and subsequent scavenging and sedimentation results in ^{210}Pb unsupported by its long-lived parent, ^{226}Ra. The decay of the unsupported ^{210}Pb over time after sedimentation and the relationship between it and other radioisotopes with depth in sediment can be used to determine the rate at which sediment is being deposited (Appleby and Oldfield, 1992). A linear sedimentation rate was estimated in each core based on ^{210}Pb decay between the two intervals (0–1 and 4–5 cm) using the constant flux-constant sedimentation (CF-CS) method (Appleby and Oldfield, 1992). Though these rates were determined from only two depth intervals and did not account for compaction of sediment, they were useful for determining relative differences in sedimentation rates and determining sites for more detailed long core analyses.

The sediment MARs (g/cm^2/a) for the long cores were determined by the CRS model (Appleby and Oldfield, 1992) from the unsupported ^{210}Pb profiles versus cumulative dry mass. To apply the model, the unsupported ^{210}Pb activity (dpm/g) for each interval is multiplied by the total mass (g/cm^3) and thickness (cm) for the interval, and summed down core. By determining a MAR for each interval from the relationship between the unsupported ^{210}Pb inventory below an interval to the whole core inventory (dpm/cm^2), the CRS model accounts for variations in MAR among intervals and for compaction. The age of each interval is calculated from the resulting MARs and cumulative mass for that interval starting at the core top. The uncertainty in MARs is determined by propagating the measurement uncertainty through the CRS model following the approach outlined in Van Metre and Fuller (2009).

Cesium-137 can be used to verify sediment age because of its well-known input history due to atmospheric fallout from nuclear weapons testing in the mid 20th century (Van Metre et al., 2004). Beryllium-7 ($t_{1/2}$ 53 days) formed in the atmosphere is used to indicate short-term deposition and/or mixing (Krishnaswami et al., 1980).

In the three long cores taken in 2006, sediments were also analyzed for 24 other trace elements. Though not discussed here, these results can be found in Oliver (2008).

3. Results and discussion

3.1. Sedimentation rates and comparison to post-Bonneville sediments

Quantifiable whole core MARs in six long cores ranged from 0.013 to 0.038 g/cm^2/a with an average of 0.027 g/cm^2/a (Table 1). These MARs are for the entire depth range of measurable unsupported ^{210}Pb and represent the average for the last ~100 a. Cores 2267 and 2565 were assigned MAR values of 0 g/cm^2/a because they failed to yield sufficient ^{210}Pb activity for MAR determination.

The decay profiles of unsupported ^{210}Pb versus cumulative dry mass and depth are shown in Fig. 2. The interpretation of the ^{210}Pb decay profiles was more straightforward for some cores than others. For example, in cores 3510, DD-L and DD-Q, the unsupported ^{210}Pb activity decreases exponentially with depth suggesting relatively constant deposition rates. In contrast, other cores, for example DD-C, DD-I and DD-R, show zones of variable ^{210}Pb activity with a subsurface maximum in ^{210}Pb activity before decreasing with depth. The zones of variable ^{210}Pb activity in these three cores could represent sediment mixing such as resuspension and redeposition; however, the absence of any detectable ^{7}Be in these cores indicates that these processes had not occurred in the few months prior to core collection. The variability and subsurface maxima are more likely the result of temporal variation in the sediment MAR, with an increase in MAR above the maxima that resulted in the decrease of ^{210}Pb activity by dilution. Due to the apparent complex depositional histories present in some of the cores, the CRS age-dating method was used to determine sediment MARs for all cores. The CRS model determines an MAR for each interval to account for the variable and nonlinear profiles of unsupported ^{210}Pb. The calculated CRS MARs for the surface 0–1 or 0–2 cm intervals (representing 5–16 a of deposition) are up to three times greater than the MAR for the whole depth range of the measurable unsupported ^{210}Pb profile (~100 a) (Table 1). The core shortening mass correction resulted in an increase in the 0–2 cm MARs of 10–30% with greater increases for cores with lower MARs. The 0–1 cm MAR in DD-Q increased by about 40% with the core shortening correction. A large increase in the CRS MAR occurs above the depth where the maximum in unsupported ^{210}Pb occurs in cores DD-C, DD-I, DD-L and DD-R. The CRS dates for these maxima are between 1972 and 1987 indicating the apparent increase in MAR started about 20–30 a ago.

The activity maximum of ^{137}Cs resulting from its well-established deposition history from the atmospheric fallout of nuclear weapons testing can also be used to verify sediment MAR. However, in this system, ^{137}Cs results were considered unreliable since most ^{137}Cs profiles exhibited a long downward tail from the surface instead of a distinct activity maximum. This is consistent with diagenetic remobilization of ^{137}Cs such as displacement from cation exchange sites on clays by NH_4^+ ions, which has been shown to occur in reducing environments (Anderson et al., 1987). This process is likely in the GSL because of the anoxic conditions within both the sediment pore waters and the water column within the deep brine layer (Domagalski, 1988). In contrast, ^{210}Pb is not significantly mobile in reducing sediments because of high sulfide concentrations. For this reason ^{137}Cs could not be used to confirm the MARs derived from ^{210}Pb profiles in these sediments.

In the south basin of the south arm of the GSL, post-Bonneville deposition (defined by the Holocene sediment thicknesses) matched the short core (<5 cm) results relatively well (Fig. 3). Areas with sediment thicknesses 2 m or less consistently showed insufficient unsupported ^{210}Pb to determine linear sedimentation rates, consistent with very low sedimentation implied by the low thickness of Holocene sediments. This very low sedimentation is also consistent with the focusing of sediments away from these sites (which are generally located in shallower areas) to deeper portions of the lake (Colman et al., 2002; Baskin, 2005). Cores located in thicker Holocene sediment (>8 m) (e.g. DD-C and DD-R) had the highest sedimentation rates (0.67 and 0.25 cm/a, respectively) derived from the ^{210}Pb decay between the two intervals in the short cores, ignoring compaction.

This agreement did not extend to the north basin of the south arm. Two short cores (DD-I and DD-H) and two long cores (2565 and DD-I) were located within this basin. Holocene sediment thicknesses at these sites indicate medium to high sedimentation rates over much of the area for the past ~10 ka (Fig. 3). However, a sedimentation rate could not be determined from cores from sites DD-H and 2565 because there was no measurable unsupported ^{210}Pb. Alternatively, the short core at site DD-I indicates higher rates of sedimentation. Though the short core results for core DD-I suggest that it may be an outlier (95 cm/a based on the 0–1 and 4–5 cm intervals), the whole core MAR determined from the long core at this location (0.038 g/cm^2/a) and the linear sedimentation rate calculated by conversion of this MAR (0.11 cm/a) are of similar magnitude to the other cores and were considered useful for this analysis.

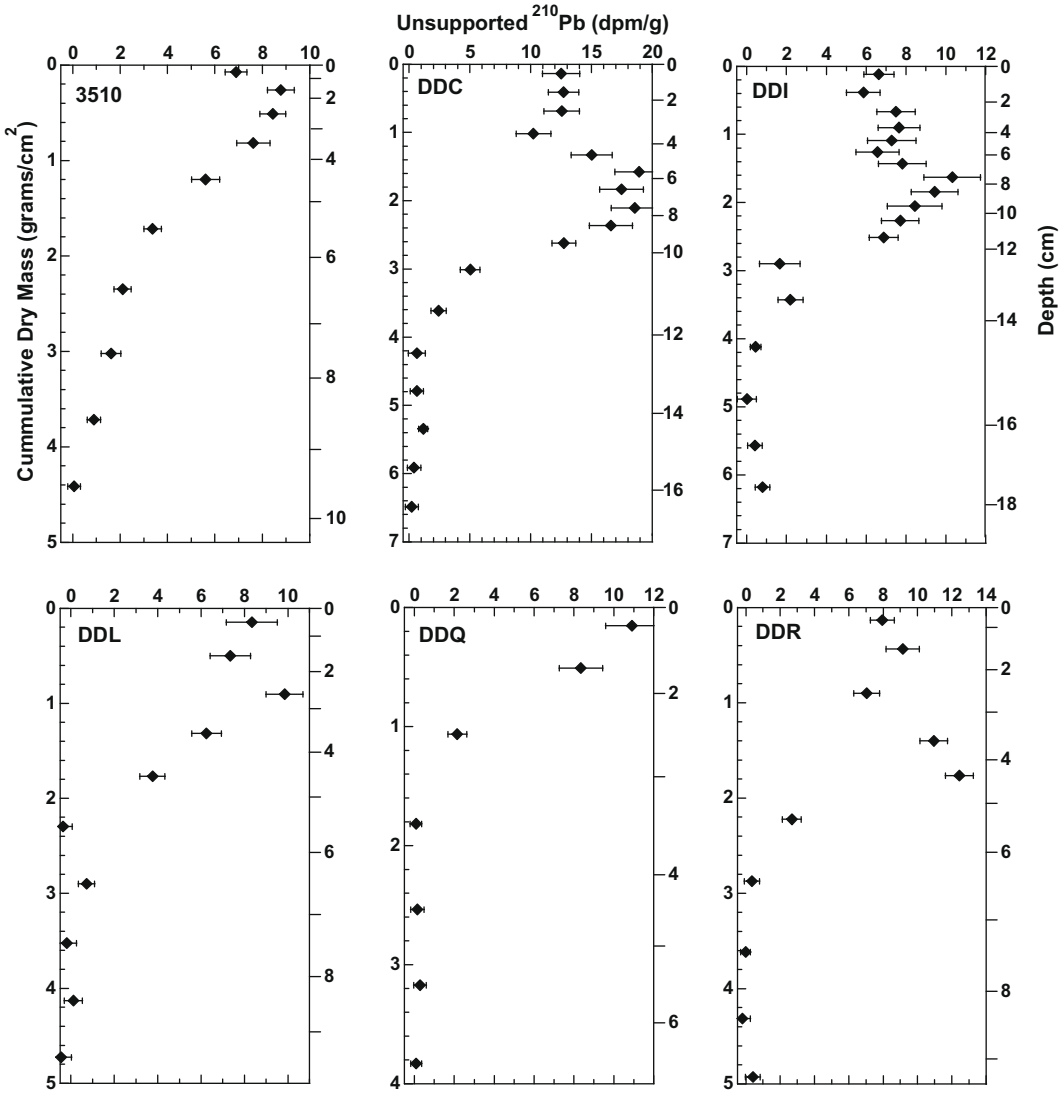

Fig. 2. Unsupported ^{210}Pb (dpm/g, salt-free) versus cumulative dry mass (g dry sediment/cm^2, salt-free) and depth (cm) in long cores. Error bars depict 1–sigma uncertainty propagated from measurement uncertainty of ^{210}Pb and its parent, ^{226}Ra.

The discrepancy between Holocene isopach contours and short core results may be due to the north basin's proximity to the railroad causeway. Prior to the construction of the causeway, the north basin of the south arm was part of a larger basin, as defined by lake bottom bathymetry, that included Gunnison Bay. Lake currents here, which are now confined by the causeway, were likely very different prior to construction (Rich, 2002). It is also possible that causeway construction activities significantly disturbed the sediment in this region by remixing sediment into the water column. The observed increase in MAR noted above for cores after the mid-1970s occurred well after construction of the causeway in 1959.

The correspondence between post-Bonneville deposition and the long cores was similar to that of the short cores, but less clear due to the limited number of long cores. Cores DD-C and DD-R, locations with thicker Holocene sediment, had high MARs relative to most of the other cores. The MARs for cores 2267 and DD-Q were very low (0 and 0.013, respectively), which is consistent with their corresponding Holocene sediment thicknesses and location in the lake. One exception is core 3510, which has a higher-than-expected whole core MAR of 0.037 g/cm^2/a relative to the Holocene sediment thickness at this location. The long cores in the north basin of the south arm also exhibited MARs that were discrepant with the underlying Holocene sediment thickness, as was observed and described above for the short cores in this area.

3.2. Sediment Se concentrations

Salinity-corrected Se concentrations for all intervals in the long cores ranged from 0.34 to 3.66 mg/kg with a mean of 1.47 mg/kg. Profiles for the Se concentrations in each of the long cores for the top 10 cm of sediment are shown in Fig. 4. Three of the eight cores show a maximum in Se concentration between 3 and 5 cm depth. Four of the eight cores also have significantly lower Se concentrations in older, deeper sediments than in the upper, more recently deposited sediments. The shape of the Se concentration profiles for cores DD-I and DD-C did not resemble the other cores, increasing steadily from approximately 1 to 3 mg/kg to a depth of 10 cm. This difference is likely because of the higher MAR in cores DD-I and DD-C and the subsequently shorter time period represented by their Se profiles. The Se concentration in cores 2267 and 2565 (MAR values of 0 g/cm^2/a) had a much lower range (0.4–1 mg/kg)

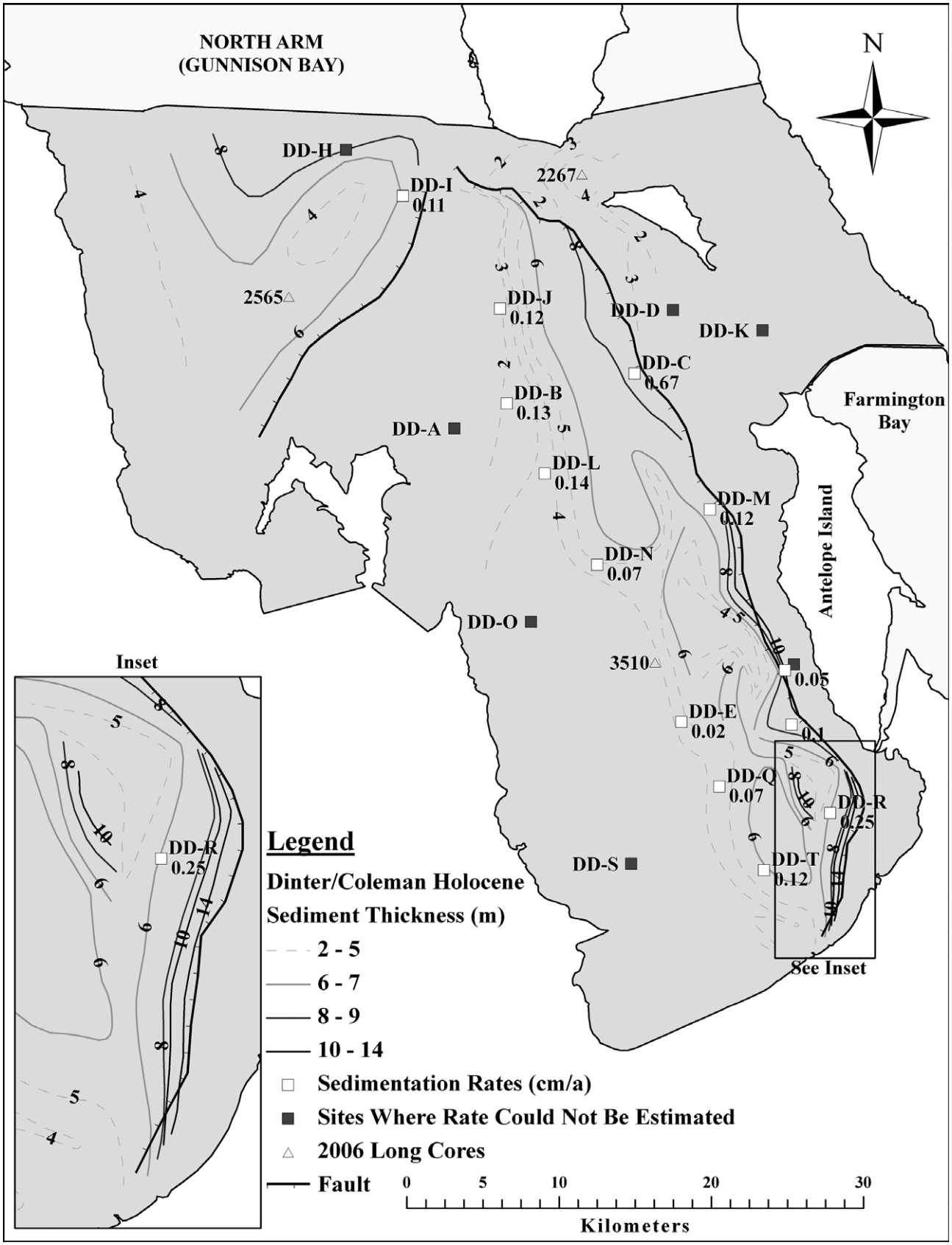

Fig. 3. Short core estimated linear sedimentation rates overlain on Holocene isopach contours. Contours developed by Dinter (2007) and Colman et al. (2002). Note: the linear sedimentation rate for core DD-I (0.11 cm/a) was estimated from long core MAR results.

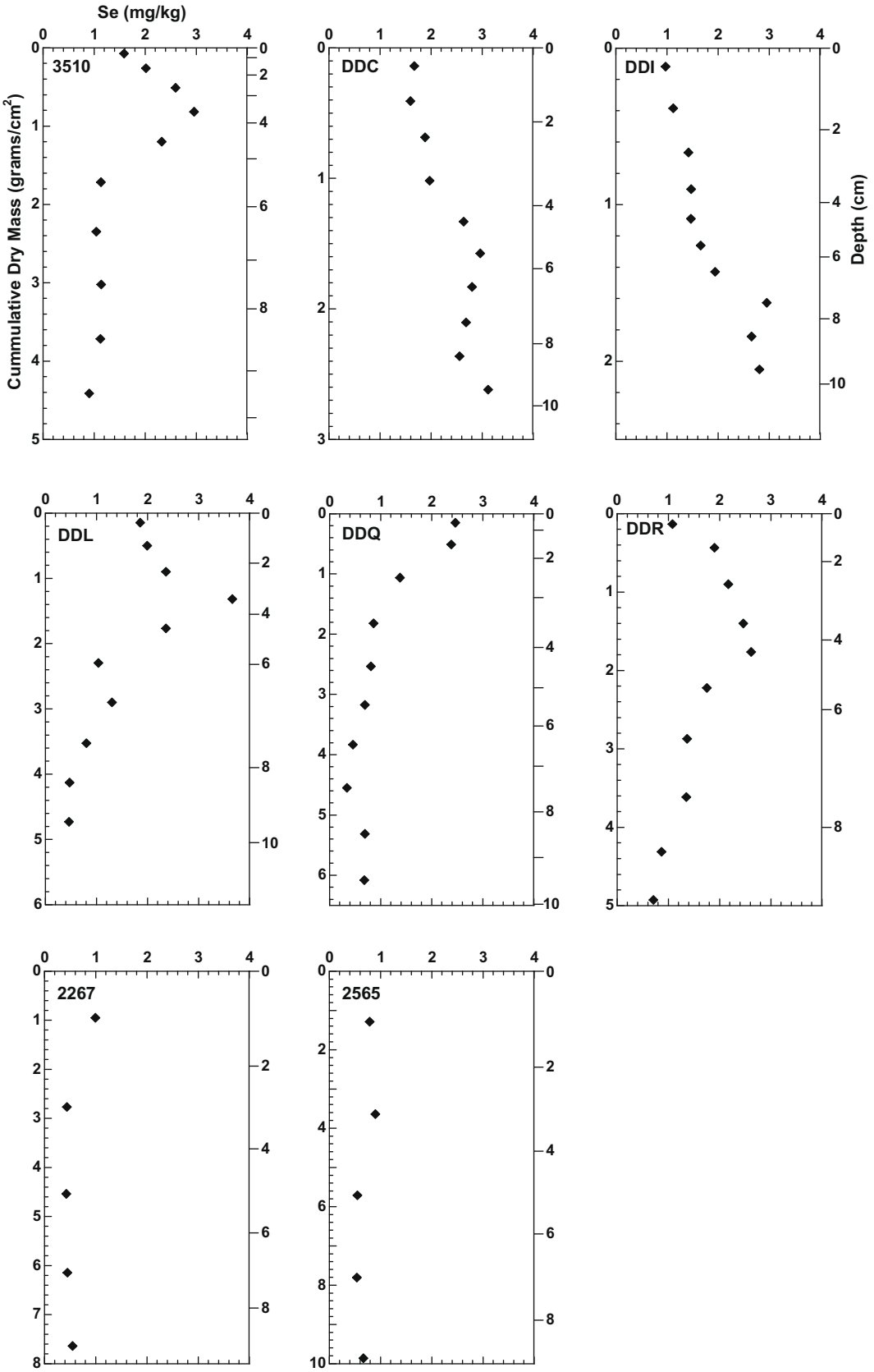

Fig. 4. Salinity-corrected Se concentration profiles in long cores versus cumulative mass (g dry sediment/cm^2) and depth (cm).

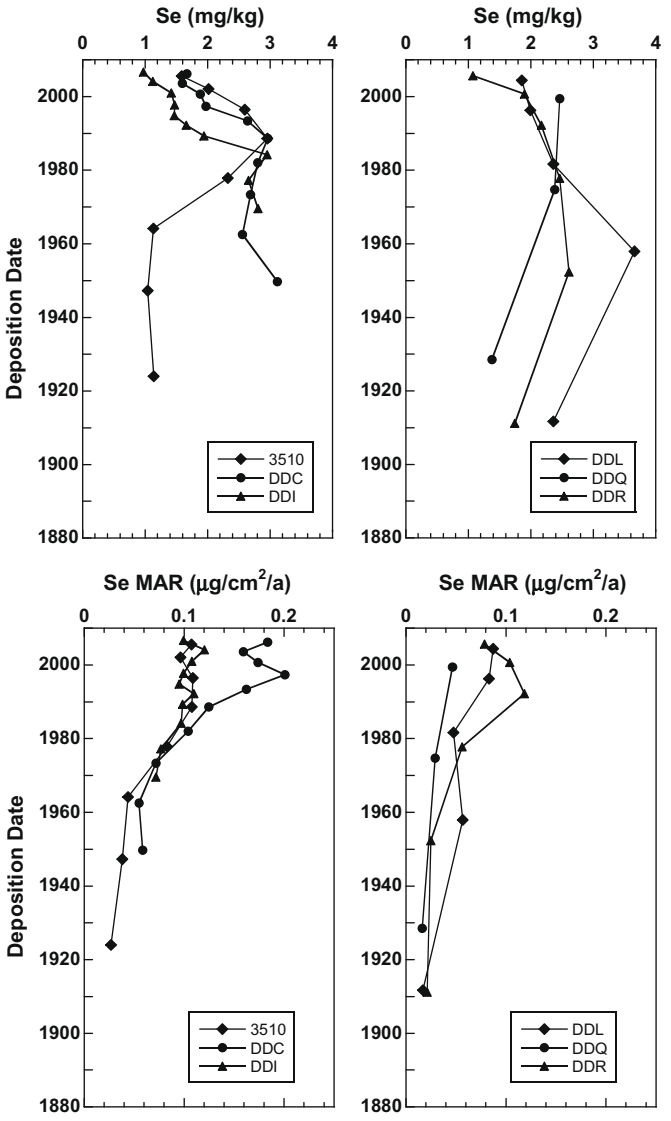

Fig. 5. Sediment salinity-corrected Se concentration and Se mass accumulation rates (Se MAR) versus date of deposition determined from ^{210}Pb CRS mass accumulation rates. Se MAR is calculated by multiplying the salinity-corrected Se concentration by the sediment mass accumulation rate for each interval.

than the other cores and exhibited little change with depth. In general, the Se concentrations in these two cores were similar to levels ($\leqslant$1 mg/kg) observed in the deeper parts of the other cores.

A chronology relating the Se concentrations in the long core sediments to the estimated date of deposition using the ^{210}Pb MAR in each core is shown in Fig. 5. Only those core intervals within the ^{210}Pb dating range are shown. Results show that, in general, the Se concentration in sediment deposited after ~1950 is 2–3 times higher than the Se concentration in sediment deposited earlier. Most cores also show a peak in concentration in the mid-to-late 20th century with Se concentration decreasing towards the surface. Although the Se profiles for cores DD-C and DD-I only extend back to 1950, the Se profiles are similar to the other cores over this time span. Calculated Se deposition rate (Se MAR), the product of the Se concentration and the sediment MAR for each interval (Fig. 5), indicates relatively stable Se MARs in each core over the past 20–30 a, except DD-R, which shows a decrease since 1990. In all cores with Se profiles extending to before 1950, the Se MAR since 1980 is a factor of 3–5 greater than the Se MAR before 1950. The increase in Se deposition rate may reflect increases in loading from natural and (or) anthropogenic inflows. For example, intermittent monitoring by the US Geological Survey of historical (1972–1984, n = 23) daily Se loads from the Kennecott Utah Copper Corporation outfall to the GSL (gage site 10172650) ranged from <1 to 30 kg/day. It is possible, however, that diagenetic processes and changes in the anoxic deep brine layer may also influence the Se concentration profile (Callender, 2000; Gwynn, 2002).

The level to which Se removal by sedimentation responds to increases in loads cannot be directly assessed because Se load estimations to the GSL are not available during this period. However, one indicator of loading to the GSL is the long-term measured discharge of tributary rivers. Annual flow from the Bear River, which flows into the NE section of the south arm of the GSL through Bear River Bay and is typically one of the largest contributors of Se load (Naftz et al., 2009), was obtained from US Geological Survey gage site 10126000 for the Bear River near Corinne, Utah. This site is the farthest downstream gage site and has a long (>50 a) record. The average annual flow rate at this site for water years 1950–2007 (October 1 through September 30) ranged from 12.3 to 143 m^3/s with a mean of 48 m^3/s. Interestingly, the four highest average discharge years (1983–1986 ranging from 87.5 to 143 m^3/s) roughly correspond to the peaks in Se concentration in sediment as a function of age presented in Fig. 5. This is most apparent in the cores with the highest whole core MARs (DD-C, DD-I and 3510) and subsequently the highest temporal resolution. The Se MARs are also higher during and after this period of high river discharge. Though this suggests that the rate of Se removal by sedimentation may be responsive to changes in loading, more research is needed to understand the dynamics of this relationship.

Chronologies for cores 2565 and 2267 are not shown because a MAR could not be determined at these locations. Both the very low activity of unsupported ^{210}Pb and the low Se concentrations in these cores (<1 mg/kg), similar to those deposited prior to 1900 in the other long cores (e.g. DD-L, DD-Q and DD-R, see Fig. 5), suggest that they represent sediment deposited significantly earlier than in the other long cores.

3.3. Estimation of Se removal by sedimentation

The mass of Se removed annually from the water column in the south arm of the GSL by sedimentation was estimated by developing qualitative sedimentation zones based primarily on the results of the 20 short cores and Holocene isopach contours, assigning an average Se concentration and MAR to each zone based on the upper 1–2 cm of the eight long cores, and summing the resulting mass of Se removed from each zone in the basin. The age represented by the averaged Se concentrations of the surface intervals in these cores ranges from 5 to 16 a of deposition, or sediment deposited no earlier than 1990 (Table 1). The thicknesses of post-Bonneville lacustrine sediment deposits were previously estimated by analysis of high-resolution seismic reflection transects (Dinter, 2007; Colman et al., 2002). Contours of this sediment, deposited during the Holocene, were plotted in ArcGIS along with the short core sedimentation rate estimates in order to develop contours delineating qualitative zones of very high to very low contemporary sedimentation rates (Fig. 3). Due to the agreement between the short core sedimentation results and the Holocene isopach contours in the south basin, the sedimentation zone boundaries were developed here by following the general shape of isopach contours while grouping together cores with similar linear sedimentation rates. The qualitative sedimentation zones developed from the relationship between short core results and Holocene sediment thickness are shown in Fig. 6.

To address the discrepancy between Holocene isopach contours and coring results in the north basin of the south arm, the coring

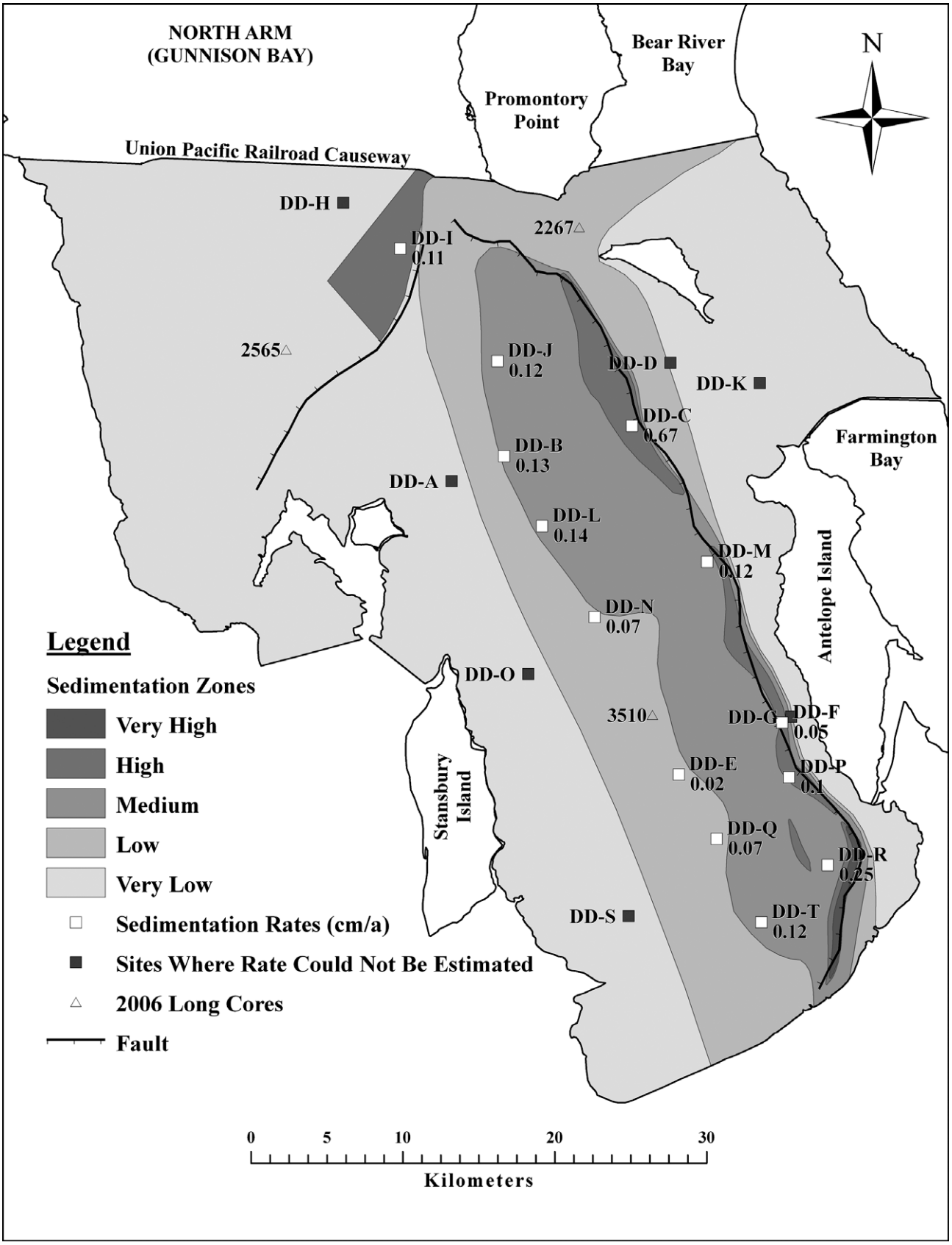

Fig. 6. Qualitative sedimentation zones based on Holocene isopach contours and short core linear sedimentation rates. Note: the linear sedimentation rate for core DD-I (0.11 cm/a) was estimated from long core MAR results.

Table 2
Area, Se concentration, mass accumulation rate (MAR), mass of Se removed annually and uncertainty in mass of Se removed annually for each qualitative sedimentation zone.

Sed region	Cores within zone	Area of zone (km^2)	RSD area	Avg. [Se] (mg/kg)	RSD avg. [Se]	MAR ($g/cm^2/a$)	RSD MAR	Mass of Se removed (kg/a)	Total zone uncertainty (kg/a)
Very low	2565	1233.2	0.083%	0.79	201%	0.00	N/A	0.00	N/A
Low	2267, 3510, DD-Q	404.6	0.083%	1.76	84%	0.02	91%	172.80	214.73
Medium	DD-L, DD-R	358.5	0.083%	1.71	53%	0.05	60%	321.51	258.75
High	DD-C	47.9	0.083%	1.64	35%	0.11	18%	82.23	32.41
High NW	DD-I	34.3	0.083%	1.05	54%	0.11	15%	37.69	21.20
Very high	none	4.6	0.083%	1.64	35%	0.13	18%	9.87	3.89
							Total	**624.11**	**±338.5**

results (both short and long cores in this case) were considered to represent contemporary sedimentation more closely than the isopach contours. Thiessen polygons were, therefore, developed around the cores for the basin bounded on the east by the SW–NE trending Carrington Fault (Colman et al., 2002). The Thiessen polygon surrounding core DD-I was designated as the "high NW" (northwest) sedimentation zone due to the relatively high MAR determined from the upper 2 cm of the long core. The polygons surrounding cores DD-H and 2565 were designated as "very low" sedimentation zones and grouped together since there was not sufficient ^{210}Pb at either of these sites to determine a sedimentation rate.

The average MAR in each zone was determined by interpretation of the surface interval MARs from the long cores (Table 1). MARs in the "medium," "high" and "high NW" zones were found by averaging the MAR values of the cores within them. The MAR for the "low" sedimentation zone was calculated by averaging the MAR values of the two cores with sufficient ^{210}Pb activity (DD-Q and 3510) with a sedimentation rate of zero for core 2267 – yielding an average MAR of 0.024 $g/cm^2/a$ (Table 2). The "very low" sedimentation zone did not contain any cores with sufficient ^{210}Pb activity to estimate a MAR. Therefore, the MAR for this zone was designated as zero. Though the area of the lake represented by the "very low" zone is large, this assignment is not considered to effect the overall removal estimation outside of the range of uncertainty. For example, if the "very low" zone was assigned an MAR of half that of the "low" zone, the result is an increase in the removal estimate by less than 20% – well within the range of uncertainty calculated below. The MAR for the "very high" sedimentation zone was estimated as 0.131 $g/cm^2/a$, 25% higher than the "high" zone value.

A representative Se concentration was also assigned to each of the zones based on the average concentration of Se in the most recently deposited sediments of the cores that fell within them (Table 2). For the "very high" sedimentation zone, the Se concentration of the nearby "high" sedimentation zone was applied. The increased uncertainty associated with this assignment was accounted for as described below. In all but one of the long cores, the average Se concentration of the top 2 cm was used to represent recent sediments. In the lone exception, core DD-Q, only the 0–1 cm interval was used because the MAR of DD-Q was much lower than that of the other cores. Since an MAR could not be determined for cores 2267 and 2565, only the topmost (0–2 cm) interval was used to represent recently deposited sediments. Though these cores likely reflect sediment deposited much earlier than in the other cores, the impact of their use on the basin-wide estimation of Se removed to sediment is minimal due to 2565 lying in a zero MAR zone and 2267 lying in a zone with two other cores used for the "low" MAR average Se concentration as well.

The average Se concentration, MAR, and area for each of the sedimentation zones described above are summarized in Table 2. The following equation was used to determine the permanent Se removal by sedimentation for each zone:

$$\mathrm{Se_{Removed}}\left(\frac{\mathrm{kg_{Se}}}{\mathrm{a}}\right) = [\mathrm{Se}]\left(\frac{\mathrm{mg}}{\mathrm{kg_{sed}}}\right) \times \mathrm{MAR}\left(\frac{\mathrm{g_{sed}}}{\mathrm{cm^2 a}}\right) \times \mathrm{Area}(\mathrm{km^2}) \times 10\left(\frac{\mathrm{kg_{sed}}}{\mathrm{g_{sed}}}\frac{\mathrm{kg_{Se}}}{\mathrm{mg_{Se}}}\frac{\mathrm{cm^2}}{\mathrm{km^2}}\right) \quad (2)$$

where $Se_{Removed}$ is the mass of Se removed per year, [Se] is the Se concentration, MAR is the mass accumulation rate, Area is the area of each sedimentation zone, and 10 is the unit correction factor. The sum of the sedimentation fluxes in each of the zones yielded the total mass of Se removed by sedimentation over the entire south arm. The resulting estimation is that about 624 kg of Se are permanently removed from the GSL by sedimentation each year.

3.4. Uncertainty in Se removal by sedimentation

Uncertainty in the annual Se mass removed by sedimentation was determined by estimating uncertainty for, and propagating uncertainty through, each step in the Se removal calculation; that is, determining the representative sediment Se concentration, MAR and area for each qualitative sedimentation zone. For the Se concentration and MAR determinations, cores with a 6.7-cm diameter were used to represent the six zones with a total area of 2083 km^2. The estimated strength of this extrapolation (i.e. the greater number of cores in each zone, the stronger the confidence in the value) was incorporated into the uncertainty calculations as described below.

In order to determine the uncertainty in the representative Se concentration for each zone, the analytical uncertainty for the Se concentration in each core slice was propagated through to the average uncertainty for the zone using the standard methods for adding uncertainties (taking the square root of the sum of the squares of the uncertainties). This process involved determining the uncertainty in the average concentration for each of the core intervals and the average of the cores that fell within each sedimentation zone.

In order to estimate the uncertainty due to extrapolating a finite number of cores to a large area, the uncertainty in the sediment Se concentration for the entire lake was first estimated as the relative standard deviation of the Se concentration of all long cores (RSD_{Lake}). This served as the background uncertainty of the entire dataset because it represents the expected distribution of sediment Se concentrations across the whole lake. This background uncertainty in Se concentration for the lake was scaled to each zone based on the relationship between the area of the zone and the number of cores used to describe it (the "area/core ratio"). The eight cores in the 2083 km^2 lake yield an area/core ratio of 260 km^2 of lake area per core. Division of RSD_{Lake} by this value, and multiplication of the quotient by the ratio of the zone area to the number of cores in that zone yielded the RSD for each zone.

The RSD for the qualitative "low" sedimentation zone is shown below as an example:

$$\mathrm{RSD}_{\text{“low”}} = \frac{45\%\ \mathrm{RSD}_{\mathrm{Lake}}}{260.4\ \mathrm{km}^2/\mathrm{core}} \times \frac{404.6\ \mathrm{km}^2}{\text{three cores}} = 23\% \quad (3)$$

The high area/core ratio in the "low" zone relative to that of the entire lake serves to decrease the uncertainty from the background of 45%, whereas a zone with a lower area/core ratio than the lake as a whole would have a higher RSD than 45%. This process was applied to all of the sedimentation zones, with the exception of the "very low" zone because the MAR and subsequent estimation of Se removal from this zone are zero and the "very high" zone because no cores fell within it. An uncertainty of 100% was applied to the "very high" zone.

To combine the uncertainties associated with Se concentration to those associated with extrapolation to larger areas, the RSDs were converted back to standard deviations and then combined as above by taking the square root of the sum of the squares of each uncertainty value.

Uncertainty in mass accumulation rate for each zone was determined using a similar method as described above for Se concentration and is based on the uncertainty estimated for each core MAR used in each zone (see above). The MAR uncertainty for each core was propagated to determine the uncertainty in the average of the core MARs within a zone. The uncertainty due to the extrapolation was then incorporated into the MAR uncertainty for each zone. Two cores (2565 and 2267) did not have an associated standard deviation because no MAR could be determined due to insufficient ^{210}Pb. For this reason, as mentioned above, an uncertainty in the MAR could not be determined for this zone. It is possible that sedimentation in this zone is not only very low, but negative, implying net erosion, as sediments are focused away from shallower areas of the lake to deeper areas of the lake. It is not possible, however, to quantify the extent to which erosion might be occurring with the currently available data. If the sedimentation rate in this zone were negative, the net result of erosion with redeposition in the higher sedimentation zones would be a decrease in the estimated mass of Se removed to sediment. The amount of reduction in the net mass of Se removed to sediment due to erosion and redeposition, if present, likely is not large because of the low Se concentration in the sediments of this zone (cores 2565 and 2267, Fig. 4). Though a MAR of zero is assigned to core 2267, an uncertainty of 0.019 was assigned to this core because this was the lowest MAR value measured among the uppermost 1–2 cm of the cores. The RSD of the "high" sedimentation zone (7.8%) was assigned to the nearby "very high" sedimentation zone because no long cores were recovered from the "very high" zone.

The uncertainty in the areal extent of each sedimentation zone was determined by scaling the uncertainty associated with the areal extent of the lake (1.73 km^2 due to a 0.03 m stage inaccuracy in the USGS gage for lake elevation) to each sedimentation zone.

It is important to note, however, that this uncertainty is three orders of magnitude less than the uncertainties for the Se concentrations and MARs and therefore does not meaningfully affect the uncertainty in the removal calculation. With uncertainties established for the sediment Se concentration, MAR and area in each zone, the uncertainty of the mass of Se removed by sedimentation was calculated using the standard method for multiplying uncertainties (square root of the sum of the squares of the RSDs). Since the masses of Se removed in each zone were summed to determine the mass removed for the lake, the uncertainty in each zone was propagated through to the final estimate by taking the square root of the sum of the squares of the uncertainty in the mass of Se removed by sedimentation from each zone. Table 2 shows the calculated uncertainty for each sedimentation zone. Results indicate that about 624 ± 338 kg of Se are permanently removed from the Great Salt Lake by sedimentation each year. This yields a range of removal of between 285 and 960 kg of Se/a when the uncertainty is included.

3.5. Implications of sedimentation to Se mass balance

Comparison of the estimation of Se removal by sedimentation with the estimation of loading of Se to the system indicates that removal by sedimentation likely accounts for less than half of the Se mass entering the main body of the GSL. Annual loading during the 12-month period of May 1st, 2006 to April 30th, 2007 was estimated to be 1560 kg of Se/a (Naftz et al., 2009). This load is well above the mean estimated Se removal by sedimentation of 624 kg and even greater than the upper estimate based on uncertainty (960 kg Se/a).

It is possible that the relationship between Se removal by sedimentation and loading could be affected by the time frames over which the estimations were developed (1 a for loading versus 5–16 a for sedimentation). However, it is unlikely that the magnitude of difference between the two estimations would be solely, or even primarily, due to this type of annual variability. Though the annual variability in Se loading to the GSL cannot be directly assessed with the data presently available, one indicator of this variability is the long-term variation in measured discharge of tributary rivers. At the US Geological Survey Bear River gage near Corinne, Utah (site 10126000) described above, the average annual flow rate for water years 1950–2007 (October 1 through September 30) ranged from 12.3 to 143 m^3/s with a mean of 48 m^3/s. The time period over which the Se loading was calculated spanned parts of water years 2006 and 2007. The average flow rate for each of these water years was 46 and 25 m^3/s, respectively. The runoff entering the south arm of the GSL for the period over which Se loading was estimated is, therefore, near or somewhat below average as gaged by the flow in the Bear River. This suggests that the loading estimate developed by Naftz et al. (2009) is likely near or somewhat below average as well.

Estimations and direct measurements of Se removal to the atmosphere indicate that volatilization, not sedimentation, is likely the main mechanism of Se removal from the GSL (Diaz et al., 2009). The mean estimate of annual Se removal by volatilization was 1455 kg/a with a range of uncertainty between 970 and 2180 kg/a.

Another significant removal mechanism for Se from the south arm of the GSL is loss to the north arm (Gunnison Bay). Naftz et al. (2009) made a preliminary estimate of 880 kg/a of Se lost to the north arm from five discrete measurements of flow at three sites along the railroad causeway.

The total estimated mass of Se removed from the south arm from the three mechanisms is almost twice the estimated loading from river inflows. Based on this, one would expect a significant decrease in the concentration of Se in the water column. However, monitoring of the Se concentration in the water column at four sites in the south arm by Naftz et al. (2009) throughout the study period showed a statistically significant (90% confidence interval) increase in the Se concentration between 0.21 and 0.33 μg/L over the 16 months from May 2006 to August 2007. This increase is equal to, or greater than, what would be expected if no removal mechanisms were occurring at all. One possible cause of this increase could be Se concentrating in the water column due to evaporation and a subsequent drop in lake volume (and water level). However, this is unlikely to be the primary cause as the lake-levels as measured at the USGS lake-level gage 10010000 at Saltair Marina drop less than 0.3 m between the overlapping months of 2006 and 2007 during the study period. This indicates a significant

unmeasured input of Se to the lake. Some possible sources of this Se, as described in Naftz et al. (2009), include unmeasured surface or groundwater inflows, dry and wet atmospheric deposition (Wen and Carignan, 2007), and aeolian deposition. Though these have the potential to be considerable sources of Se to the GSL, the significance of each is not currently known. The relationship between loading and removal mechanisms and the implications thereof are discussed in more detail in Diaz et al. (2009).

4. Summary and conclusions

A series of sediment cores was collected during the summers of 2006 and 2007 across the south arm of the GSL to estimate the annual rate of Se removal by sedimentation. Three long cores were collected during 2006. Twenty short cores were then taken during the summer of 2007 in order to guide the selection of locations for five additional long cores collected the next month. The short cores were analyzed for linear sedimentation rate from analysis of ^{210}Pb decay between two depths. Sediment mass accumulation rates (MARs) in the long cores were determined using the CRS method. Selenium concentration was measured in the upper 10 cm of the long cores.

Whole core MARs in the eight long cores ranged from 0.013 to 0.038 g/cm^2/a with a mean of 0.027 g/cm^2/a. Two long cores (2565 and 2267), however, did not have measurable ^{210}Pb activity to allow determination of a MAR, indicating very low or possibly negative rates of sedimentation at these locations.

In general, in the south basin of the south arm, the variation in sediment MARs and linear sedimentation rates among sites agreed well with the thickness of sediment deposited during the Holocene as determined in Colman et al. (2002) and Dinter (2007). This agreement did not extend, however, to the north basin of the south arm. The proximity of the north basin of the south arm to the railroad causeway and activities associated with its construction in the 1950s may have contributed to this disagreement.

Selenium concentrations in the eight long cores ranged from 0.34 to 3.66 mg/kg with a mean of 1.47 mg/kg (Figs. 4 and 5). Many cores exhibited a peak in Se deposited in the latter half of the 20th century, especially between 1970 and 1990.

The linear sedimentation rates and MARs were used along with the thickness of Holocene sediment to develop qualitative zones of very high to very low sedimentation rates across the south arm of the GSL. Based on the long cores, an average MAR and Se concentration was determined for each of the sedimentation zones in order to estimate the total mass of Se removed to sediment in the south arm of the GSL annually. Results indicate that approximately 624 kg of Se are removed annually within a range of uncertainty of 285–960 kg of Se. The uncertainty range was determined by propagating uncertainty through each step in the estimation calculation and included uncertainty due to extrapolation.

An estimate of Se loading to the GSL from riverine inflows by Naftz et al. (2009) of 1560 kg of Se/a indicates that sedimentation removes less than half of the Se loaded to the system. An estimate of Se removal by volatilization by Diaz et al. (2009) of 1455 kg of Se per year indicates that volatilization, not sedimentation, dominates as a removal mechanism. The imbalance of removal processes to loads, coupled with a statistically significant increase in the water column concentration of Se in the GSL, suggests that there may be significant unmeasured loads of Se to the south arm of the GSL.

This estimate of Se removed from the south arm of the GSL by sedimentation indicates that sedimentation is a significant, but not the primary removal mechanism for Se from the GSL.

Acknowledgements

The authors gratefully acknowledge Jennifer Wilson and Christopher Braun, USGS, Austin, Texas, for their assistance in collecting, processing, and analyzing the sediment cores. In addition the authors would like to thank Peter Van Metre, Ryan Rowland, Patrick Lambert and an anonymous journal peer reviewer for their thoughtful and helpful comments and suggestions. This research was funded by the Utah Dept. of Environmental Quality, a GK-12 Grant through the National Science Foundation, and the US Geological Survey. Use of brand names in this publication does not constitute endorsement by either the University of Utah or the US Geological Survey.

References

Aldrich, T.W., Paul, D.S., 2002. Avian ecology of Great Salt Lake. In: Gwynn, J.W. (Ed.), Great Salt Lake: An Overview of Change. Utah Department of Natural Resources, pp. 343–374.

Amouroux, D., Donard, O.F.X., 1996. Maritime emissions of selenium to the atmosphere in Eastern Mediterranean seas. Geophys. Res. Lett. 23, 1777–1780.

Amouroux, D., Donard, O.F.X., 1997. Evasion of selenium to the atmosphere via biomethylation processes in the Gironde Estuary, France. Mar. Chem. 58, 173–188.

Anderson, R.A., Schiff, S.L., Hesslein, R.H., 1987. Determining sediment accumulation and mixing rates using ^{210}Pb, ^{137}Cs and other tracers: problems due to postdepositional mobility or coring artifacts. Can. J. Fish. Aquat. Sci. 44 (s1), s231–s250.

Appleby, P.G., Oldfield, F., 1992. Application of ^{210}Pb to sedimentation studies. In: Ivanovich, M., Harmon, R.S. (Eds.), Uranium-series Disequilibrium: Application to Earth Marine, and Environmental Sciences, second ed. Claredon Press, Oxford, pp. 731–778 (Chapter 21).

Baskin, R.L., 2005. Calculation of area and volume for the south part of the Great Salt Lake, Utah. US Geol. Surv., Open-File Rep. 2005–1327USGS.

Blomqvist, S., 1985. Reliability of core sampling of soft bottom sediment – an in situ study. Sedimentology 32, 605–612.

Callender, E., 2000. Geochemical effects of rapid sedimentation in aquatic systems: minimal diagenesis and the preservation of historical metal signatures. J. Paleolimnol. 23, 243–260.

Colman, S.M., Kelts, K.R., Dinter, D.A., 2002. Depositional history and neotectonics in Great Salt Lake, Utah, from high-resolution seismic tomography. Sediment. Geol. 148, 61–78.

Crusius, J.C., Anderson, R.F., 1991. Core compression and surficial sediment loss of lake sediments of high porosity caused by gravity coring. Limnol. Oceanogr. 36, 1021–1031.

Diaz, X., Johnson, W.P., Oliver, W., Naftz, D.L., 2009. Volatile selenium flux from the Great Salt Lake, Utah. Environ. Sci. Technol. 43, 53–59.

Dinter, D., 2007. Suggested core sample locations in the Great Salt Lake based on long-term Holocene depositional rates estimated from chirp and geopulse seismic reflection profiles. Pers. Comm.

Domagalski, J.K., 1988. Trace metal and organic geochemistry of closed basin lakes. Ph.D. Thesis, Johns Hopkins Univ.

Gwynn, J.W., 2002. Chemical and physical variations of the brine and effects of the SPRR causeway. In: Gwynn, J.W. (Ed.), Great Salt Lake: An Overview of Change. Utah Dept. of Natural Resources, pp. 87–106.

Heinz, G.H., 1996. Selenium in birds. In: Beyer, W.N., Heinz, G.H., Redmon-Norwood, A.W. (Eds.), Environmental Contaminants in Wildlife – Interpreting Tissue Concentrations. Lewis Publishers, Boca Raton, Florida, pp. 447–458.

Keith, J.O., 2005. An overview of the American White Pelican. Waterbirds 28, 9–17 (Special Publication 1).

Krishnaswami, S., Benninger, L.K., Aller, R.C., Von Damm, K.L., 1980. Atmospherically-derived radionuclides as tracers of sediment mixing and accumulation in near-shore marine and lake sediments: evidence from ^{7}Be, ^{210}Pb, and ^{239,240}Pu. Earth Planet. Sci. Lett. 47, 307–318.

Mahler, B.J., Van Metre, P.C., Callender, E., 2006. Trends in metals in urban and reference lake sediments across the United States, 1970 to 2001. Environ. Toxicol. Chem. 25 (7), 1698–1709.

Naftz, D.L., Stephens, D.W., Callender, E., Van Metre, P.C., 2000. Reconstructing historical changes in the environmental health of watersheds by using sediment cores from lakes and reservoirs in Salt Lake Valley, Utah. US Geol. Surv, Fact Sheet FS-164-00.

Naftz, D.L., Johnson, W.P. Freeman, M., Beisner, K., Diaz, X., Cross, V.A., 2009. Estimation of selenium loads entering the south arm of Great Salt Lake, Utah, from May 2006 through March 2008. US Geol. Surv. Scient. Invest. Rep. 2008-5069.

Nriagu, J.O., 1989. A global assessment of natural sources of atmospheric trace metals. Nature 338, 47–49.

Ohlendorf, H.M., 2003. Ecotoxicology of selenium. In: Hoffman, D.J., Rattner, B.A., Burton, G.A., Jr., Cairns, J.C., Jr. (Eds.), Handbook of Ecotoxicology, second ed. Lewis Publishers, pp. 465–500.

Oliver, W., 2008. Selenium removal processes from Great Salt Lake, UT: estimating sedimentation and verifying volatilization fluxes. Masters Thesis, Univ. Utah.

Rich, J., 2002. Great Salt Lake south arm circulation: currents, velocities, and influencing factors. In: Gwynn, J.W. (Ed.), Great Salt Lake: An Overview of Change. Utah Dept. of Natural Resources, pp. 171–183.

Seiler, R.L., Skorupa, J.P., Naftz, D.L., Nolan, B.T., 2003. Irrigation-induced contamination of water, sediment, and biota in the western United States – synthesis of data from the National Irrigation Water Quality Program. US Geol. Surv. – Prof. Paper 1655.

Shussman, B., 1999. Wilson's Phalarope. Wildlife Notebook Series No. 6, Utah Division of Wildlife Resources.

Stokes, W.L., 1980. Geologic setting of Great Salt Lake. In: Gwynn, J.W. (Ed.), Great Salt Lake: A Scientific, Historical, and Economic Overview. Utah Geological and Mineral Survey Bull., vol. 116, pp. 55–68.

Sturm, P.A., 1980. The Great Salt Lake brine system. In: Gwynn, J.W. (Ed.), Great Salt Lake: A Scientific, Historical, and Economic Overview. Utah Geological and Mineral Survey Bull., vol. 116, pp. 147–162.

Tayler, P.L., Hutchinson, L.A., Muir, M.K., 1980. Heavy metals in the Great Salt Lake, Utah. In: Gwynn, J.W. (Ed.), Great Salt Lake: A Scientific, Historical, and Economic Overview. Utah Geological and Mineral Survey Bull., vol. 116, pp. 195–200.

Van Metre, P.C., Fuller, C.C., 2009. Dual-core mass-balance approach for evaluating mercury and ^{210}Pb atmospheric fallout and focusing to lakes. Environ. Sci. Technol. 43, 26–32.

Van Metre, P.C., Wilson, J.T., Fuller, C.C., Callender, E., Mahler, B.J., 2004. Collection, analysis, and age-dating of sediment cores from 56 US lakes and reservoirs sampled by the US Geological Survey, 1992–2001. US Geol. Surv. Scient. Invest. Rep. 2004-5184.

Wen, H., Carignan, J., 2007. Reviews on atmospheric selenium: emissions, speciation, and fate. Atmos. Environ. 41, 7151–7165.

Wurtsbaugh, W., 2007. Preliminary analyses of selenium bioaccumulation in benthic food webs of the Great Salt Lake, Utah. In: Final Report: Development of a Selenium Standard for the Open Waters of the Great Salt Lake. Utah Department of Environmental Quality.